



**HAL**  
open science

## South African speleothems reveal influence of high- and lowlatitude forcing over the past 113.5 k.y.

Brian M. Chase, Chris Harris, Maarten de Wit, Jan Kramers, Sean Doel,  
Jacek Stankiewicz

### ► To cite this version:

Brian M. Chase, Chris Harris, Maarten de Wit, Jan Kramers, Sean Doel, et al.. South African speleothems reveal influence of high- and lowlatitude forcing over the past 113.5 k.y.. *Geology*, 2021, 10.1130/G49323.1 . hal-03312173

**HAL Id: hal-03312173**

**<https://hal.science/hal-03312173>**

Submitted on 2 Aug 2021

**HAL** is a multi-disciplinary open access archive for the deposit and dissemination of scientific research documents, whether they are published or not. The documents may come from teaching and research institutions in France or abroad, or from public or private research centers.

L'archive ouverte pluridisciplinaire **HAL**, est destinée au dépôt et à la diffusion de documents scientifiques de niveau recherche, publiés ou non, émanant des établissements d'enseignement et de recherche français ou étrangers, des laboratoires publics ou privés.

1 South African speleothems reveal influence of high- and low-  
2 latitude forcing over the last 113.5 kyr

3  
4 The authors do not recommend the distribution of this version  
5 of this article.

6 The article is freely available upon request.

7 To receive a copy, please send a request to Brian Chase at:  
8 [brian.chase@umontpellier.fr](mailto:brian.chase@umontpellier.fr)

9  
10 **Brian Chase<sup>1,2</sup>, Chris Harris<sup>3</sup>, Maarten J de Wit<sup>4</sup>, Jan Kramers<sup>5</sup>, Sean Doel<sup>3,6</sup> and Jacek**  
11 **Stankiewicz<sup>7</sup>**

12 *<sup>1</sup>Institut des Sciences de l'Evolution-Montpellier (ISEM), University of Montpellier, Centre*  
13 *National de la Recherche Scientifique (CNRS), EPHE, IRD, 34095 Montpellier, France*

14 *<sup>2</sup>Department of Environmental and Geographical Science, University of Cape Town, South Lane,*  
15 *Upper Campus, 7701 Rondebosch, South Africa*

16 *<sup>3</sup>Department of Geological Sciences, University of Cape Town, 7700 Rondebosch, South Africa*

17 *<sup>4</sup>AEON & Earth Stewardship Science Research Institute, Nelson Mandela University, 6031 Port*  
18 *Elizabeth, South Africa*

19 *<sup>5</sup>Department of Geology, University of Johannesburg, 2006 Johannesburg, South Africa*

20 *<sup>6</sup>WSP, Environment & Energy, 8001 Cape Town, South Africa*

21 *<sup>7</sup>European Center for Geodynamics and Seismology, Rue Josy Welter, 19*  
22 *L-7256 Walferdange, Luxembourg*

23 **ABSTRACT**

24 Variation in  $\delta^{18}\text{O}$  and  $\delta^{13}\text{C}$  values in a speleothem from the Cango Caves in southernmost South  
25 Africa enable the construction of coherent regional composite records spanning the last 113,500  
26 years. Novel for the region in terms of both their length and detail, these records indicate  
27 environmental and climatic changes that are both consistent with records from the wider region  
28 and show a clear evolution from low- to high latitude forcing dominance across the last glacial  
29 period. Prior to  $\sim 70$  ka, the influence of direct low latitude insolation forcing is expressed through  
30 increases in summer rainfall during austral summer insolation maxima. With the onset of Marine  
31 Isotope Stage 4, cooler global conditions and the development of high latitude ice sheets appear to  
32 have supplanted direct insolation forcing as the dominant driver pacing patterns of environmental  
33 change, with records from the Southern and Northern Hemisphere tropics exhibiting a positive  
34 relationship until after the Last Glacial Maximum. These results highlight the complexity of South  
35 African climate change dynamics as a response to changing global boundary conditions and  
36 provide a critical reference for regional and global comparisons.

37

38 **INTRODUCTION**

39 Terrestrial proxy records of past environmental change in southern Africa are spatially and  
40 temporally restricted. The region's semi-arid to arid climates do not favour the development of  
41 natural lakes and wetlands, and long, continuous terrestrial palaeoenvironmental records are rare  
42 (see review by Chase and Meadows, 2007). This fundamental limitation becomes increasingly  
43 acute with age, with few records spanning Marine Isotope Stages (MIS) 3-5. As a result, little is  
44 known about climate and environmental dynamics in South Africa during the last glacial period.  
45 Existing records indicate the transient dominance of both 1) direct low-latitude orbital forcing  
46 (Partridge et al., 1997) and 2) high northern latitudes forcing, as transmitted to southern Africa via  
47 atmospheric and oceanic teleconnections (Chase et al., 2015; Chevalier and Chase, 2015; Schefuß  
48 et al., 2011). Lacking, however, is a basis to study how regional climates and environments  
49 responded to the changing global boundary conditions that were associated with the transition from  
50 interglacial to glacial climates. This is a period is of particular importance in South Africa because  
51 it represents a crucial time for human cultural and technological evolution, including the Still Bay  
52 and Howiesons Poort industries (Jacobs et al., 2008). To date, without sufficiently detailed, reliable  
53 records, it has not been possible to establish a firm link between these episodes and potential  
54 environmental forcing factors.

55 In this paper, we address this issue with the oxygen and carbon isotope stratigraphy of a  
56 1.5 m stalagmite from the Cango Caves (Fig. 1, SI1), a cave site that has provided seminal records  
57 that have been fundamental to our understanding of southern African palaeoenvironments (Talma  
58 and Vogel, 1992). Encompassing the period from 40.1-106 ka, we use  $\delta^{18}\text{O}$  and  $\delta^{13}\text{C}$  records from  
59 the stalagmite as lynchpins to use reduced major axis (RMA) regression to establish regional  
60 composite records (Fig. 2) including previously published data from the site (Talma and Vogel,

61 1992), data from the nearby site of Efflux Cave (Braun et al., 2020) and – for  $\delta^{13}\text{C}$  – rock hyrax  
62 middens from Seweweekspoort (Chase et al., 2017) (Fig. 1) (for further information regarding  
63 materials, methods and results supporting the details and discussion provided here, please refer to  
64 the Supplementary Information). These composite  $\delta^{18}\text{O}$  and  $\delta^{13}\text{C}$  records span the last 113.5 kyr  
65 and are used to explore the nature and dynamics of environmental change and its drivers across  
66 the last interglacial-glacial transition and last glacial cycle.

## 67 **REGIONAL SETTING**

68 The Cango Caves (Fig. 1, SI1) form a string of interconnected sub-horizontal linear caverns, some  
69 2.5 km long, within deformed Proterozoic limestone of the Groot Swartberg Mountains of South  
70 Africa. The cave system is formed below a Cretaceous-Cenozoic paleo-denudation surface. The  
71 vegetation at Cango Caves is Kango Limestone Renosterveld (Rebelo et al., 2006), a grassy  
72 shrubland dominated by renosterbos (*Elytropappus rhinocerotis*) and shrubs and grasses of both  
73  $\text{C}_3$  and  $\text{C}_4$  varieties (Vogel, 1978). Crassulacean Acid Metabolism (CAM) plants (many  
74 succulents) including *Aloe* spp. and succulent shrubs (particularly Crassulaceae) can be abundant  
75 in the region. Climate in South Africa is broadly determined by two dominant climate systems, the  
76 tropical easterlies which advect moist air off the warm southwestern Indian Ocean during the  
77 summer months, and frontal systems embedded in the westerly storm track that bring rain to the  
78 southwestern Cape and southern Cape coast during the winter months (Tyson, 1986) (Fig. 1).  
79 Spatial distinctions in rainfall regimes across the subcontinent have given rise to the classification  
80 of a winter rainfall zone (WRZ), an aseasonal or year-round rainfall zone (ARZ or YRZ) and a  
81 summer rainfall zone (SRZ) (sensu Chase and Meadows, 2007). The Cango Caves are located in  
82 the modern ARZ, receiving ~48% of its mean annual rainfall in the winter months (MJJAS)  
83 (Hijmans et al., 2005).

84 **DISCUSSION**

85 In general, variability in speleothem calcite  $\delta^{18}\text{O}$  values ( $\delta^{18}\text{O}_c$ ) is controlled by cave temperature  
86 and the  $\delta^{18}\text{O}$  of the rainwater percolating into the cave. Rainwater  $\delta^{18}\text{O}$  values ( $\delta^{18}\text{O}_p$ ) are governed  
87 by a series of inter-related ‘effects’ (Dansgaard, 1964), namely temperature, source, continentality  
88 and the “amount effect”, the latter of which is particularly significant in tropical regions, such as  
89 South Africa’s summer rainfall zone (Herrmann et al., 2017). In South Africa’s winter rainfall  
90 zone, lower  $\delta^{18}\text{O}_p$  is associated with cooler, wetter winter months and stratiform rainfall (Aggarwal  
91 et al., 2016; Harris et al., 2010; IAEA/WMO, 2020). Considering South Africa’s position – and  
92 particularly that of the study region – at the dynamic interface between tropical and temperate  
93 climate regimes (Chase et al., 2017; Chevalier and Chase, 2015; Schefuß et al., 2011), each of  
94 these effects and factors are likely to have influenced regional  $\delta^{18}\text{O}_c$  records, and parsing them –  
95 and the influence of other effects - to isolate distinct controls has proven to be generally intractable  
96 (see Holmgren et al., 2003) particularly over the time periods considered here.

97 Variability in speleothem calcite  $\delta^{13}\text{C}$  ( $\delta^{13}\text{C}_c$ ) primarily reflects changes in the aggregate  
98  $\delta^{13}\text{C}$  value of the soil organics (Fohlmeister et al., 2020), which in turn depends primarily on the  
99 plant’s photosynthetic pathway ( $\text{C}_3$ , ~-34 to -24‰;  $\text{C}_4$ , ~-16 to -10‰ and CAM, ~-20 to -10‰)  
100 (O’Leary, 1988; Smith and Epstein, 1971). Of these,  $\text{C}_3$  plants are generally trees and shrubs as  
101 well as grasses that grow in cool to cold environments,  $\text{C}_4$  plants are primarily grasses adapted to  
102 warm growing seasons, and CAM represents an adaptation to water stress. As mentioned, plants  
103 of each type currently exist in the study region, and their proportions have been demonstrated to  
104 vary in the past as a function of changing climate (Sealy et al., 2016). Other factors, such as  
105 changes in vegetation density (and thus soil respiration), and prior carbonate precipitation are  
106 considered unlikely to have had significant influence on the  $\delta^{13}\text{C}_c$  records as the nature of the

107 regional vegetation types (Rebelo et al., 2006), the amplitude of regional temperature changes  
108 (Chase and Meadows, 2007), and the lack of correlation between  $\delta^{13}\text{C}_c$  and speleothem growth  
109 rates (Fohlmeister et al., 2020) are not conducive to, or consistent with, significant variability  
110 related to such factors.

111 Across the last 113.5 kyr, the CFC  $\delta^{13}\text{C}$  record highlights the influence of temperature on  
112 regional vegetation, with cooler global temperatures generally corresponding with less  $\text{C}_4$  grass  
113 (Fig. 2). This relationship, however, evolves as a function of changing global boundary conditions.  
114 Prior to the onset of Marine Isotope Stage 4 (MIS 4) at  $\sim 70$  ka, CFC  $\delta^{13}\text{C}$  variability is consistent  
115 with orbital precession, with the most compelling comparison existing with the precipitation  
116 reconstruction from Tswaing Crater (Fig. 1, 2). Located  $\sim 1000$  km to the northeast of the Cango  
117 Caves in the summer rainfall zone, the Tswaing Crater record has been presented as evidence for  
118 the influence of direct insolation forcing in southern Africa (Partridge et al., 1997), and the CFC  
119  $\delta^{13}\text{C}$  record indicates increases in  $\text{C}_4$  grass prevalence during periods of increased summer rainfall.

120 The CFC  $\delta^{13}\text{C}$  record provides corroboration for the results and interpretation of the Tswaing  
121 Crater record and together they enable a more reliable basis for comparison with other records  
122 from further afield. Of particular interest are records from the Northern Hemisphere tropics that  
123 can be used to assess the nature and dynamics of direct precessional forcing since the eccentricity  
124 maximum at 115 ka (Laskar et al., 2004). Of these, a  $\delta\text{D}$  record from leaf waxes from marine core  
125 RC09-166 in the Gulf of Aden (Tierney et al., 2017) provides the clearest reflection of northeast  
126 African tropical hydroclimate over this time period. Consistent with predictions based on direct  
127 precession-paced insolation forcing (Partridge et al., 1997), the period from 115 ka to  $\sim 70$  ka is  
128 characterized by an antiphase relationship between patterns of precipitation change in the  
129 northeastern and southeastern African tropics (Fig. 2e). However, with declining eccentricity the

130 negative correlation between Northern and Southern Hemisphere records diminishes with the onset  
131 of MIS 4. From ~70 ka to the beginning of the Holocene, Tswaing Crater and the Gulf of Aden  
132 record exhibit a strong positive correlation at precessional timescales, indicating a dominant  
133 influence of Northern Hemisphere high latitude forcing throughout this period (Fig. 2e). The  
134 change in CFC  $\delta^{13}\text{C}$  likely reflects a change from summer to winter rainfall dominance in the  
135 Congo region. The more progressive nature of the change in relationship between the CFC  $\delta^{13}\text{C}$   
136 record and the northern tropics may reflect the influence of cooler temperatures on regional  
137 vegetation following the onset of MIS 4 or a dynamic specific to changes in summer vs. winter  
138 rainfall regimes at the distal margin of the summer rainfall zone (Fig.1).

139 The trend from low- to high latitude dominance is also evident in the comparison of the CFC  
140  $\delta^{18}\text{O}_c$  record and the composite  $\delta^{18}\text{O}_c$  record from Chinese speleothems reflecting Asian monsoon  
141 dynamics and the impact of global climate change on low northern latitudes (Cheng et al., 2016).  
142 Highlighted again is a strong negative correlation prior to the onset of MIS 4, and a transition to a  
143 strong positive relationship with the shift to high latitude dominance (Fig. 2). The timing and  
144 nature of CFC  $\delta^{18}\text{O}_c$  anomalies prior to ~70 ka correlate well both with 1) increased summer  
145 insolation and precipitation at Tswaing Crater as well as 2) proxies for more extensive Antarctic  
146 sea-ice (Fischer et al., 2007) (Fig. 2), which may have displaced the westerlies storm track  
147 equatorward, resulting in increased winter rainfall in the region (Chase et al., 2017). However,  
148 coeval increases in CFC  $\delta^{13}\text{C}_c$  (more  $\text{C}_4$  grasses) indicate that these phases of lower CFC  $\delta^{18}\text{O}_c$  are  
149 most likely the result of more/more regular summer rain (Fig. 2), and suggest limitations in  
150 interpretive models that ascribe lower  $\delta^{18}\text{O}_c$  values to increased proportions of winter rain (Braun  
151 et al., 2020), as this would generally result in lower  $\delta^{13}\text{C}$  values.

152 While CFC  $\delta^{18}\text{O}$  variability after ~70 ka is consistent with variability in Greenland ice cores  
153 reflecting temperature variability during MIS 4-2 (Rasmussen et al., 2014)(Fig. 2), and the nature  
154 of the CFC  $\delta^{18}\text{O}$  record during this period would be consistent with changes in cave temperature,  
155 extending this interpretation of Talma and Vogel (1992) (reconstructed by estimating the  $\delta^{18}\text{O}$  of  
156 past precipitation using groundwater  $\delta^{18}\text{O}$  values from the nearby Uitenhage Aquifer) cannot be  
157 reliably established without a more complete record of past precipitation  $\delta^{18}\text{O}$ . Other explanations  
158 could relate to an increase in the influence of winter rainfall associated with the strong increase in  
159 Antarctic sea-ice at the onset of MIS 3 (~57 ka) (Fischer et al., 2007)(Fig. 2) and a displacement  
160 of the frontal systems and predominantly stratiform rainfall (generally lower  $\delta^{18}\text{O}_p$ ; Aggarwal et  
161 al., 2016) associated with the mid-latitude westerlies storm track. This would indicate a change  
162 from summer to winter rainfall dominance across MIS 4, but – as this relationship is not maintained  
163 after the onset of MIS 2 (~29 ka) – more work remains to be done to adequately contextualize and  
164 understand the long-term variability of - and influences on -  $\delta^{18}\text{O}_c$  in the region.

165 The MIS 4 transition from low- to high latitude dominance is also concurrent with the Still  
166 Bay and Howiesons Poort lithic industries (Fig. 2). Finding no clear relationship with Antarctic  
167 temperature records, Jacobs et al. (2008) concluded these industries could not be explained by  
168 environmental factors alone. While not establishing a comprehensive case for how  
169 environment/climatic conditions acted as a driver of the Still Bay and Howiesons Poort, the CFC  
170 records do show that each industry is associated with episodes of environmental change, likely  
171 periods of cooler conditions with decreased summer rainfall (Fig. 2). The records presented here  
172 cannot on their own define the nature of the relationship between environmental and cultural  
173 change, but they do provide a much clearer framework within which more comprehensive models  
174 may be established.

175 **CONCLUSIONS**

176 New speleothem  $\delta^{13}\text{C}$  and  $\delta^{18}\text{O}$  records from the Cango Caves have enabled the construction of  
177 regional composite records that highlight important aspects of the evolution of South African  
178 climate across the last glacial period. Prior to  $\sim 70$  ka, direct low latitude insolation forcing is the  
179 primary driver of orbital scale climate variability, as expressed by peaks in summer rainfall and  
180 the development of more extensive  $\text{C}_4$  grass cover during phases of relative aridity in the Northern  
181 Hemisphere tropics (Fig. 2). After  $\sim 70$  ka, under decreasing orbital eccentricity and with the  
182 development of more extensive high latitude ice sheets, high latitude forcing becomes the  
183 dominant driver of climate change, with strong positive relationships and a synchronous  
184 relationship being established between the Northern and Southern Hemisphere tropics at orbital  
185 timescales.

186 **ACKNOWLEDGMENTS**

187 We thank Hein Gerstner the Chief Scientific Officer of the Cango Caves for support in 1995, and  
188 the National Monuments Council for permission to remove the stalagmite. Fayrooza Rawoot  
189 helped with the C and O isotope analyses. This work was funded through various grants of the  
190 National Research Foundation (NRF) to MDW and CH. We would also like to thank the editor  
191 and two anonymous reviewers for their constructive suggestions.

192 **REFERENCES CITED**

- 193 Aggarwal, P. K., Romatschke, U., Araguas-Araguas, L., Belachew, D., Longstaffe, F. J., Berg,  
194 P., Schumacher, C., and Funk, A., 2016, Proportions of convective and stratiform  
195 precipitation revealed in water isotope ratios: *Nature Geoscience*, v. 9, no. 8, p. 624-629.  
196 Bar-Matthews, M., Marean, C. W., Jacobs, Z., Karkanas, P., Fisher, E. C., Herries, A. I. R.,  
197 Brown, K., Williams, H. M., Bernatchez, J., Ayalon, A., and Nilssen, P. J., 2010, A high  
198 resolution and continuous isotopic speleothem record of paleoclimate and  
199 paleoenvironment from 90 to 53 ka from Pinnacle Point on the south coast of South  
200 Africa: *Quaternary Science Reviews*, v. 29, no. 17-18, p. 2131-2145.  
201 Braun, K., Bar-Matthews, M., Matthews, A., Ayalon, A., Cowling, R. M., Karkanas, P., Fisher,  
202 E. C., Dyez, K., Zilberman, T., and Marean, C. W., 2019, Late Pleistocene records of

203 speleothem stable isotopic compositions from Pinnacle Point on the South African south  
204 coast: *Quaternary Research*, v. 91, no. 1, p. 265-288.

205 Braun, K., Bar-Matthews, M., Matthews, A., Ayalon, A., Zilberman, T., Cowling, R. M., Fisher,  
206 E. C., Herries, A. I. R., Brink, J. S., and Marean, C. W., 2020, Comparison of climate and  
207 environment on the edge of the Palaeo-Agulhas Plain to the Little Karoo (South Africa)  
208 in Marine Isotope Stages 5–3 as indicated by speleothems: *Quaternary Science Reviews*,  
209 v. 235, p. 105803.

210 Chase, B. M., Boom, A., Carr, A. S., Carré, M., Chevalier, M., Meadows, M. E., Pedro, J. B.,  
211 Stager, J. C., and Reimer, P. J., 2015, Evolving southwest African response to abrupt  
212 deglacial North Atlantic climate change events: *Quaternary Science Reviews*, v. 121, no.  
213 0, p. 132-136.

214 Chase, B. M., Chevalier, M., Boom, A., and Carr, A. S., 2017, The dynamic relationship between  
215 temperate and tropical circulation systems across South Africa since the last glacial  
216 maximum: *Quaternary Science Reviews*, v. 174, p. 54-62.

217 Chase, B. M., and Meadows, M. E., 2007, Late Quaternary dynamics of southern Africa's winter  
218 rainfall zone: *Earth-Science Reviews*, v. 84, no. 3-4, p. 103-138.

219 Cheng, H., Edwards, R. L., Sinha, A., Spötl, C., Yi, L., Chen, S., Kelly, M., Kathayat, G., Wang,  
220 X., Li, X., Kong, X., Wang, Y., Ning, Y., and Zhang, H., 2016, The Asian monsoon over  
221 the past 640,000 years and ice age terminations: *Nature*, v. 534, p. 640.

222 Chevalier, M., and Chase, B. M., 2015, Southeast African records reveal a coherent shift from  
223 high- to low-latitude forcing mechanisms along the east African margin across last  
224 glacial–interglacial transition: *Quaternary Science Reviews*, v. 125, p. 117-130.

225 Cooper, G. R. J., and Cowan, D. R., 2008, Comparing time series using wavelet-based  
226 semblance analysis: *Computers & Geosciences*, v. 34, no. 2, p. 95-102.

227 Dansgaard, W., 1964, Stable isotopes in precipitation.: *Tellus*, v. 16, p. 436-447.

228 Fischer, H., Fundel, F., Ruth, U., Twarloh, B., Wegner, A., Udisti, R., Becagli, S., Castellano, E.,  
229 Morganti, A., Severi, M., Wolff, E., Littot, G., Röthlisberger, R., Mulvaney, R., Hutterli,  
230 M. A., Kaufmann, P., Federer, U., Lambert, F., Bigler, M., Hansson, M., Jonsell, U., de  
231 Angelis, M., Boutron, C., Siggaard-Andersen, M.-L., Steffensen, J. P., Barbante, C.,  
232 Gaspari, V., Gabrielli, P., and Wagenbach, D., 2007, Reconstruction of millennial  
233 changes in dust emission, transport and regional sea ice coverage using the deep EPICA  
234 ice cores from the Atlantic and Indian Ocean sector of Antarctica: *Earth and Planetary  
235 Science Letters*, v. 260, no. 1–2, p. 340-354.

236 Fohlmeister, J., Voarintsoa, N. R. G., Lechleitner, F. A., Boyd, M., Brandtstätter, S., Jacobson,  
237 M. J., and L. Oster, J., 2020, Main controls on the stable carbon isotope composition of  
238 speleothems: *Geochimica et Cosmochimica Acta*, v. 279, p. 67-87.

239 Harris, C., Burgers, C., Miller, J., and Rawoot, F., 2010, O- and H-isotope record of Cape Town  
240 rainfall from 1996 to 2008, and its application to recharge studies of Table Mountain  
241 groundwater, South Africa: *South African Journal of Geology*, v. 113, no. 1, p. 33-56.

242 Herrmann, N., Boom, A., Carr, A. S., Chase, B. M., West, A. G., Zabel, M., and Schefuß, E.,  
243 2017, Hydrogen isotope fractionation of leaf wax n-alkanes in southern African soils:  
244 *Organic Geochemistry*, v. 109, p. 1-13.

245 Hijmans, R., Cameron, S. E., Parra, J. L., Jones, P. G., and Jarvis, A., 2005, Very high resolution  
246 interpolated climate surfaces for global land areas: *International Journal of Climatology*,  
247 v. 25, p. 1965-1978.

248 Holmgren, K., Lee-Thorp, J. A., Cooper, G. R. J., Lundblad, K., Partridge, T. C., Scott, L.,  
249 Sitaldeen, R., Talma, A. S., and Tyson, P. D., 2003, Persistent millennial-scale climatic  
250 variability over the past 25,000 years in Southern Africa: *Quaternary Science Reviews*, v.  
251 22, p. 2311-2326.

252 IAEA/WMO, 2020, Global Network of Isotopes in Precipitation. The GNIP Database.

253 Jacobs, Z., Roberts, R. G., Galbraith, R. F., Deacon, H. J., Grun, R., Mackay, A., Mitchell, P.,  
254 Vogelsang, R., and Wadley, L., 2008, Ages for the Middle Stone Age of southern Africa:  
255 implications for human behavior and dispersal: *Science*, v. 322, no. 5902, p. 733-735.

256 Jouzel, J., Masson-Delmotte, V., Cattani, O., Dreyfus, G., Falourd, S., Hoffmann, G., Minster,  
257 B., Nouet, J., Barnola, J. M., Chappellaz, J., Fischer, H., Gallet, J. C., Johnsen, S.,  
258 Leuenberger, M., Loulergue, L., Luethi, D., Oerter, H., Parrenin, F., Raisbeck, G.,  
259 Raynaud, D., Schilt, A., Schwander, J., Selmo, E., Souchez, R., Spahni, R., Stauffer, B.,  
260 Steffensen, J. P., Stenni, B., Stocker, T. F., Tison, J. L., Werner, M., and Wolff, E. W.,  
261 2007, Orbital and millennial Antarctic climate variability over the past 800,000 years.:  
262 *Science*, v. 317, p. 793-797.

263 Laskar, J., Robutel, P., Joutel, F., Gastineau, M., Correia, A. C. M., and Levrard, B., 2004, A  
264 long-term numerical solution for the insolation quantities of the Earth: *A&A*, v. 428, no.  
265 1, p. 261-285.

266 O'Leary, M. H., 1988, Carbon isotopes in photosynthesis: *Bioscience*, v. 38, no. 5, p. 328-336.

267 Partridge, T. C., deMenocal, P. B., Lorentz, S. A., Paiker, M. J., and Vogel, J. C., 1997, Orbital  
268 forcing of climate over South Africa: a 200,000-year rainfall record from the Pretoria  
269 Saltpan: *Quaternary Science Reviews*, v. 16, no. 10, p. 1125-1133.

270 Quick, L. J., Meadows, M. E., Bateman, M. D., Kirsten, K. L., Mäusbacher, R., Haberzettl, T.,  
271 and Chase, B. M., 2016, Vegetation and climate dynamics during the last glacial period  
272 in the fynbos-afrotemperate forest ecotone, southern Cape, South Africa: *Quaternary*  
273 *International*, v. 404, Part B, p. 136-149.

274 Rasmussen, S. O., Bigler, M., Blockley, S. P., Blunier, T., Buchardt, S. L., Clausen, H. B.,  
275 Cvijanovic, I., Dahl-Jensen, D., Johnsen, S. J., Fischer, H., Gkinis, V., Guillevic, M.,  
276 Hoek, W. Z., Lowe, J. J., Pedro, J. B., Popp, T., Seierstad, I. K., Steffensen, J. P.,  
277 Svensson, A. M., Vallelonga, P., Vinther, B. M., Walker, M. J. C., Wheatley, J. J., and  
278 Winstrup, M., 2014, A stratigraphic framework for abrupt climatic changes during the  
279 Last Glacial period based on three synchronized Greenland ice-core records: refining and  
280 extending the INTIMATE event stratigraphy: *Quaternary Science Reviews*, v. 106, p. 14-  
281 28.

282 Rebelo, A. G., Boucher, C., Helme, N., Mucina, L., and Rutherford, M. C., 2006, Fynbos Biome,  
283 *in* Mucina, L., and Rutherford, M. C., eds., *The Vegetation of South Africa, Lesotho and*  
284 *Swaziland*: Pretoria, South African National Biodiversity Institute, p. 53-219.

285 Reynolds, R. W., Smith, T. M., Liu, C., Chelton, D. B., Casey, K. S., and Schlax, M. G., 2007,  
286 Daily High-Resolution-Blended Analyses for Sea Surface Temperature: *Journal of*  
287 *Climate*, v. 20, no. 22, p. 5473-5496.

288 Schefuß, E., Kuhlmann, H., Mollenhauer, G., Prange, M., and Pätzold, J., 2011, Forcing of wet  
289 phases in southeast Africa over the past 17,000 years: *Nature*, v. 480, no. 7378, p. 509-  
290 512.

291 Sealy, J., Lee-Thorp, J., Loftus, E., Faith, J. T., and Marean, C. W., 2016, Late Quaternary  
292 environmental change in the Southern Cape, South Africa, from stable carbon and

293 oxygen isotopes in faunal tooth enamel from Boomplaas Cave: *Journal of Quaternary*  
294 *Science*, v. 31, no. 8, p. 919-927.  
295 Smith, B. N., and Epstein, S., 1971, Two categories of  $^{13}\text{C}/^{12}\text{C}$  ratios for higher plants: *Plant*  
296 *Physiology*, v. 47, p. 380-384.  
297 Talma, A. S., and Vogel, J. C., 1992, Late Quaternary paleotemperatures derived from a  
298 speleothem from Cango Caves, Cape Province, South Africa: *Quaternary Research*, v. 37,  
299 no. 2, p. 203-213.  
300 Tierney, J. E., deMenocal, P. B., and Zander, P. D., 2017, A climatic context for the out-of-  
301 Africa migration: *Geology*, v. 45, no. 11, p. 1023-1026.  
302 Tyson, P. D., 1986, *Climatic Change and Variability in Southern Africa*, Cape Town, Oxford  
303 University Press.  
304 Vogel, J. C., 1978, Isotopic assessment of the dietary habits of ungulates: *South African Journal*  
305 *of Science*, v. 74, no. 8, p. 298-301.  
306  
307

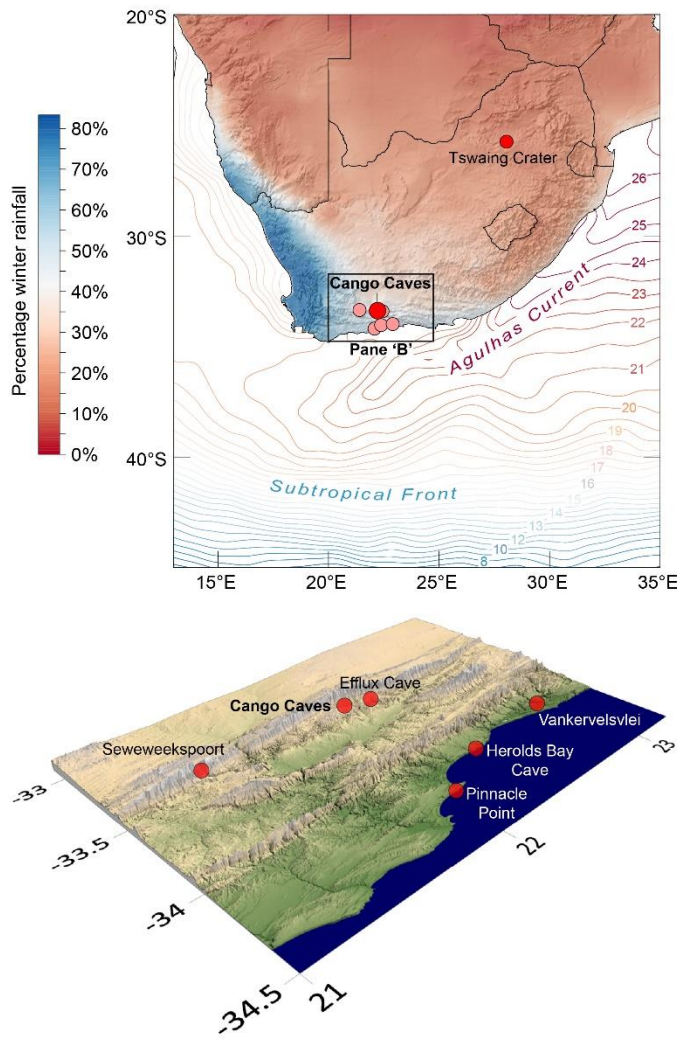


**Figure 1.** Map of southern Africa and study region, including sites considered and other records spanning marine isotope stage 4 and 5 from the region (Bar-Matthews et al., 2010; Braun et al., 2019; Braun et al., 2020; Chase et al., 2017; Partridge et al., 1997; Quick et al., 2016; Talma and Vogel, 1992). Map shading reflects modern rainfall seasonality (Hijmans et al., 2005) across the subcontinent provided as percentage of annual precipitation falling in winter months (here defined as April-September). Ocean contours reflect sea-surface temperatures in °C (Reynolds et al., 2007).

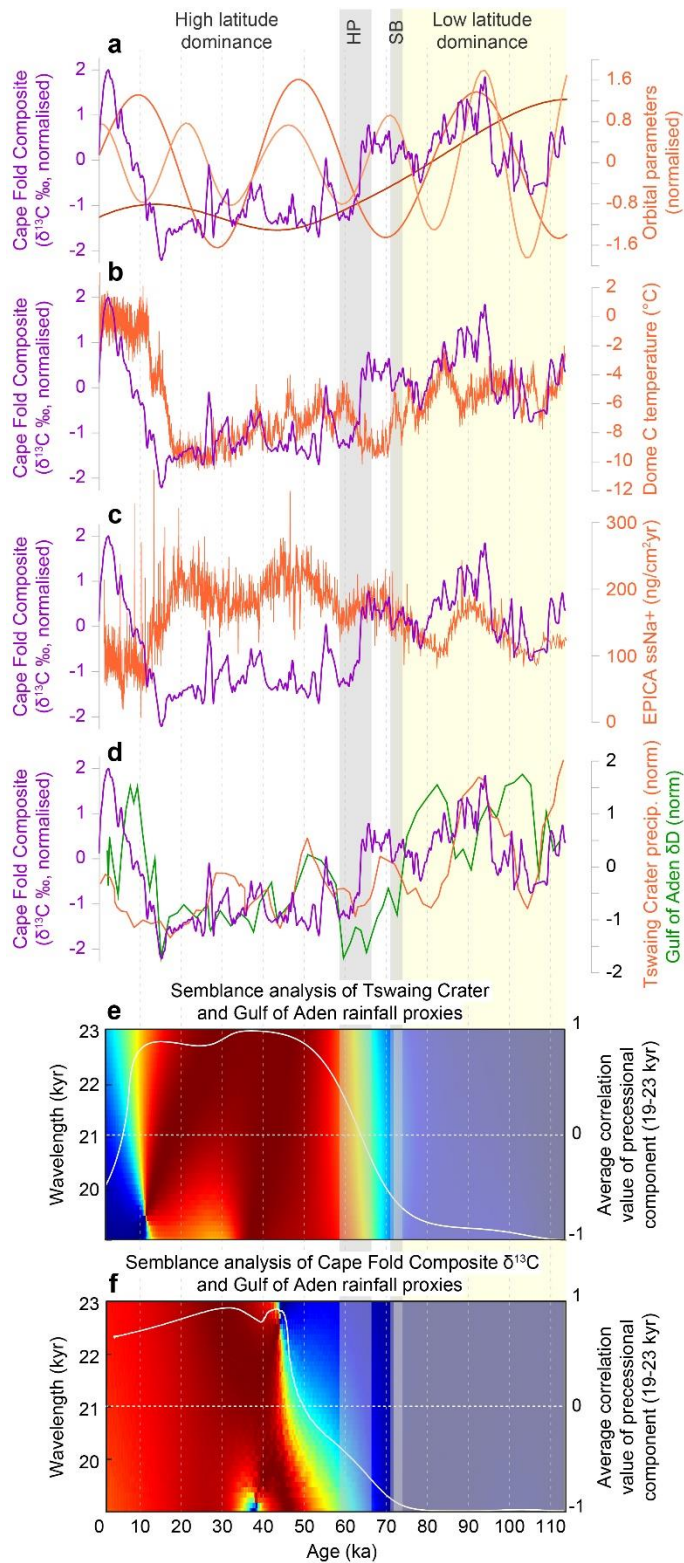


**Figure 2.** Comparison of the Cape Fold Composite calcite  $\delta^{13}\text{C}$  record with **a)** orbital parameters (eccentricity, obliquity and summer (DJF) insolation at  $25^\circ\text{S}$ ) (Laskar et al., 2004), **b)** the Dome C Antarctic temperature record (Jouzel et al., 2007), **c)** the Antarctic sea-salt sodium flux record (Fischer et al., 2007), and **d)** the hydroclimate proxies from Tswaing Crater, South Africa (Partridge et al., 1997) and the Gulf of Aden ( $\delta\text{D}$  values multiplied by  $-1$  for comparability with Tswaing Crater record; Tierney et al., 2017). The results of semblance analyses (Cooper and Cowan, 2008; red indicates a semblance of  $+1$  (positive correlation), and blue indicates a semblance of  $-1$  (negative correlation)) of the precessional component of **e)** the Tswaing Crater and **f)** the Cape Fold Composite calcite  $\delta^{13}\text{C}$  record and Gulf of Aden  $\delta\text{D}$  record indicate the transition from low to high

346 latitude forcing at ~70 ka. Grey shaded zones indicate the timing and duration of the Still Bay  
347 and Howiesons Poort lithic industries (Jacobs et al., 2008).

348

349

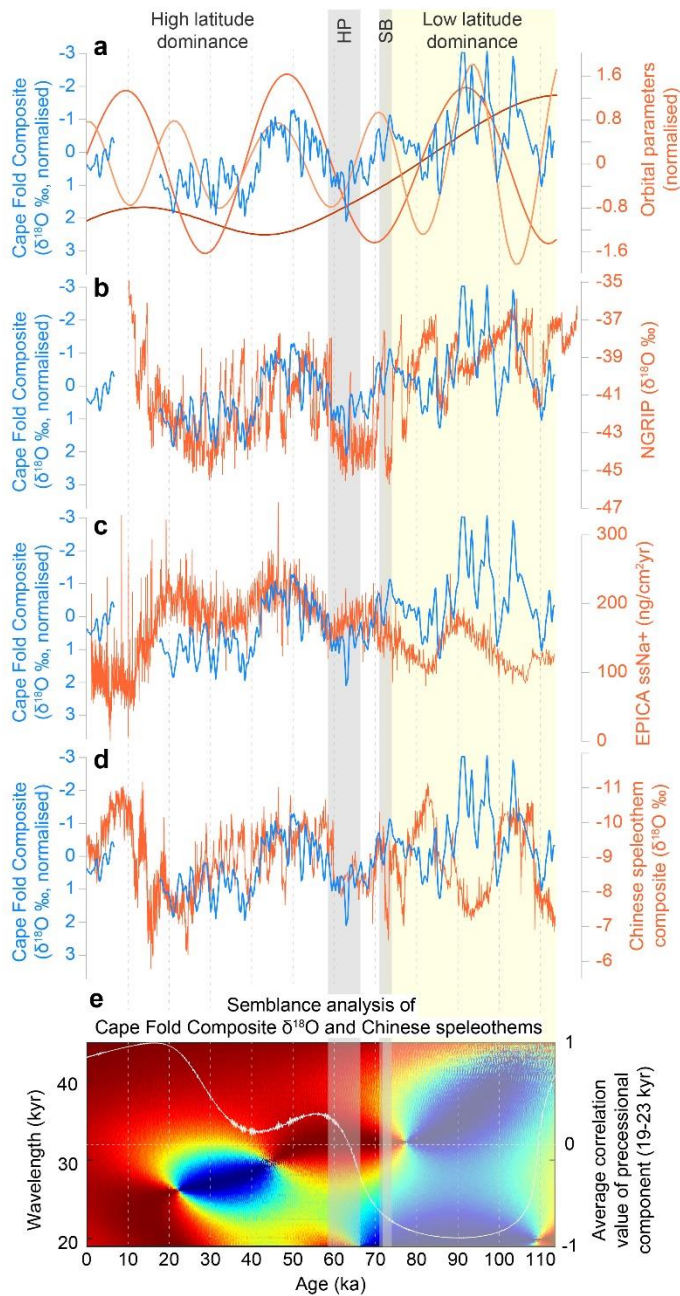


**Figure 3.** Comparison of the Cape Fold Composite calcite  $\delta^{18}\text{O}$  record with **a**) orbital parameters (eccentricity, obliquity and summer (DJF) insolation at  $25^\circ\text{S}$ ) (Laskar et al., 2004), **b**) the Greenland NGRIP  $\delta^{18}\text{O}$  record (Rasmussen et al., 2014), **c**) the Antarctic sea-salt sodium flux record (Fischer et al., 2007), and **d**) the composite  $\delta^{18}\text{O}$  record from Chinese speleothems (Cheng et al., 2016). The results of semblance analyses (**e**) (Cooper and Cowan, 2008; red indicates a semblance of +1 (positive correlation), and blue indicates a semblance of -1 (negative correlation)) of the precessional and obliquity components of Cape Fold Composite and Chinese speleothem  $\delta^{18}\text{O}$  records (Cheng et al., 2016) indicate the transition from low to high latitude forcing at  $\sim 70$  ka. Grey shaded zones indicate the timing and duration of the Still Bay and Howiesons Poort lithic industries (Jacobs et al., 2008).

# South African speleothems reveal influence of high- and lowlatitude forcing over the past 113.5 k.y.

## SUPPLEMENTARY INFORMATION

### MATERIALS

The Congo Caves (33.39°S, 22.21°E) comprises a 4 km system of chambers. In 1995, a 1.55 m tall stalagmite (CAN1) was collected ~750 m from the main Cave entrance (Fig. SI1). The caves are situated in limestone that is part of the Kango Supergroup, a Neoproterozoic siliciclastic-carbonate sequence that crops out between the steep southern early Palaeozoic Table Mountain Group of the mountain range to the north, and the flat semi-arid plains of the Oudtshoorn Basin to the south, which comprises a thick, coarse terrestrial siliciclastic ‘molasse’ sequence of Jurassic to Cretaceous age. Earlier work on the speleothems from the Congo Caves are reported by Talma and Vogel (1992) and Vogel and Kronfeld (1997).

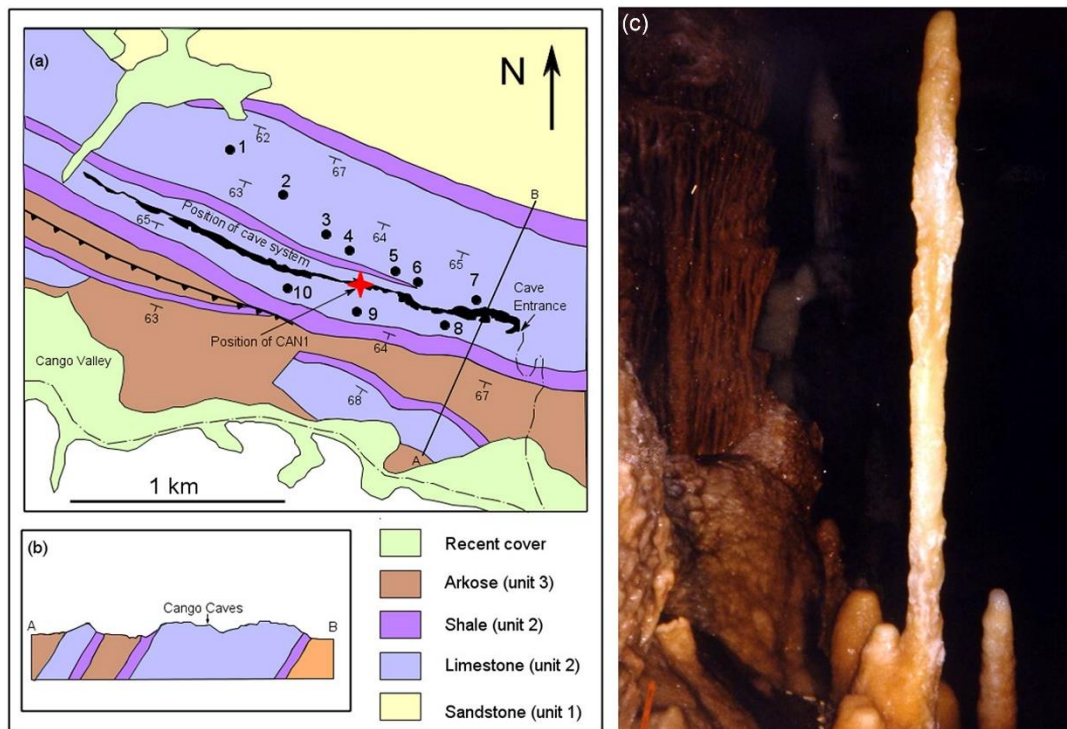


Figure SI1: Location of speleothem CAN1 in the Congo Caves system (a), regional geology (b), the CAN1 speleothem in-situ (c). Numbers = surface rock samples (SAM prefix Table SI1). Map from Doel (1995) and cave system from South African Speleological Association (1978).

Table S11: Surface rock sample stable carbon and oxygen isotope results. Location of samples corresponds to numbers in Figure S11.

<b>Country rock - Matjies River Formation</b>				
Sample		$\delta^{13}\text{C}$	$\delta^{18}\text{O}$ SMOW	$\delta^{18}\text{O}$ PDB
SAM2		0.89	24.39	-6.32
SAM3		-4.31	25.23	-5.51
SAM4		-0.69	26.23	-4.54
SAM5		2.25	27.22	-3.58
SAM7		-0.55	26.37	-4.40
SAM8		-0.61	25.60	-5.15
SAM9		1.31	26.73	-4.05
SAM10		2.71	23.47	-7.22

## METHODS

CAN1 was transported to the laboratory at the University of Cape Town and cut into six pieces of equal length and then each cut in half lengthwise using a diamond tipped rotary saw. Samples for U-series dating ( $n=21$ , 0.2-0.36 g, Table S12) were sent to the University of Bern, Switzerland for analysis. All analysed samples come from the central axis of the stalagmite. The carbonate in CAN1 is extremely pure and no solid residue, or cloudiness in the acid, remained after dissolution in phosphoric acid.

Samples for carbon and oxygen isotope analysis (20-25 mg each) were taken every 5 cm as close as possible the central axis of each stalagmite and parallel to the growth rings, using a 2 mm drill bit. 110 samples of CAN1 were analysed at the University of Cape Town. The sampling of the CAN1 speleothem reflects the techniques of the day, and combined with the brittle nature of the calcite, much of the CAN1 speleothem was destroyed in the sampling process.

Samples were analysed using both off-line and standard gas-bench techniques. Off-line extraction of  $\text{CO}_2$  from carbonates was made using the method of McCrea (1950) with 100% phosphoric acid. Samples were reacted at  $25^\circ\text{C}$  and a  $\text{CO}_2$ -calcite fractionation factor of 1.01025 was used to correct the raw data. C and O isotope ratios were measured using either a Finnegan MAT252 or a Thermo XP mass spectrometer. An internal calcite standard (NM;  $\delta^{13}\text{C} = 1.57\text{‰}$ ,  $\delta^{18}\text{O} = 25.10\text{‰}$  relative to PDB and SMOW, respectively) calibrated using NBS-19 was used to normalize raw data to the SMOW and PDB scales. Repeat analysis of the NM standard suggests that the precision is 0.2 and 0.1‰ for  $\delta^{18}\text{O}$  and  $\delta^{13}\text{C}$ , respectively. Samples were reacted at  $70^\circ\text{C}$  using the on-line gas bench analysed along with the standards Lincoln Limestone, NBS18 and NBS20, which have a range of  $\delta^{13}\text{C}$  and  $\delta^{18}\text{O}$  values. The measured and accepted values were used to construct a calibration curve and this was used to correct the raw data, and to determine the precision of the method. Repeated analyses of the standards suggest that the  $\delta^{13}\text{C}$  and  $\delta^{18}\text{O}$  values are accurate to within 0.14‰ and 0.18‰ ( $2\sigma$ ), respectively.

## RESULTS

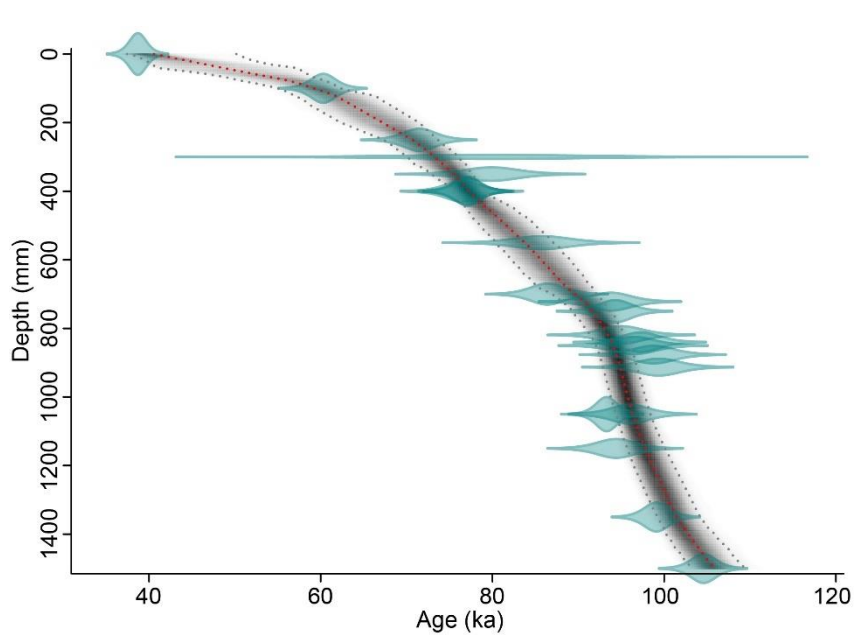
### Uranium-series dating and age model development

Table. SI2: Cango Caves speleothem U-series dating results. Activity ratios calculated using the decay constants for  $^{234}\text{U}$  and  $^{230}\text{Th}$  determined by Cheng et al. (2013). Values/yr:  $^{234}\text{U}$  ( $2.8222 \pm 0.0030$ )E-6 and  $^{230}\text{Th}$  ( $9.1706 \pm 0.01335$ )E-6. For samples with significant Th/U ratios (Table B), corrections applied in Table A are based on the assumption that the "detrital fraction" has a Th/U ratio similar to that of average continental crust (4.2) and has U-series nuclides in secular equilibrium. Detrital fractions rarely have Th/U ratios lower than 4.2, and these corrections are the maximum to be expected.

<b>TABLE A</b>													
Sample name	Dist, mm	ppb U	ppb Th	Activity ratios ( $^{230}\text{Th}/^{238}\text{U}$ )	$\pm$ 1SE	( $^{234}\text{U}/^{238}\text{U}$ )	$\pm$ 1SE	( $^{230}\text{Th}/^{234}\text{U}$ )	$\pm$ 1SE	App. Age (ka)	$\pm$ 95%	( $^{234}\text{U}/^{238}\text{U}$ ) init.	$\pm$ 95%
CAN 1- 1	0	68.7	7.4	1.174	0.001	3.006	0.015	0.391	0.003	<b>38.7</b>	0.9	3.24	0.03
CAN 1- 3	100	76.8	2.6	1.389	0.001	3.097	0.005	0.448	0.004	<b>60.3</b>	1.3	3.49	0.02
CAN 1- 6 R	250	40.6	0.8	1.351	0.002	2.640	0.009	0.512	0.004	<b>71.5</b>	1.7	3.01	0.02
CAN 1- 7	300	44.0	3.4	1.474	0.009	2.654	0.006	0.556	0.024	<b>80.3</b>	9.3	3.08	0.06
CAN 1- 8	350	36.2	2.3	1.489	0.003	2.688	0.006	0.554	0.007	<b>79.9</b>	2.8	3.12	0.02
CAN 1- 9 R	400	39.5	0.5	1.516	0.002	2.814	0.007	0.539	0.005	<b>76.5</b>	1.8	3.25	0.02
K 9	400	48.5	n.d	1.453	0.005	2.697	0.006	0.539	0.003	<b>77.0</b>	1.4	3.11	0.01
CAN 1- 12	550	27.3	0.3	1.572	0.003	2.692	0.016	0.584	0.007	<b>85.8</b>	2.9	3.16	0.04
CAN 1- 15 R	700	54.6	0.2	1.560	0.002	2.661	0.007	0.586	0.005	<b>86.4</b>	1.8	3.12	0.02
CAN 1-15 B	722	55.3	10.0	1.688	0.012	2.715	0.007	0.622	0.005	<b>93.8</b>	2.1	3.23	0.02
CAN 1-16	750	56.3	4.4	1.685	0.012	2.700	0.004	0.624	0.004	<b>94.3</b>	1.7	3.22	0.02
CAN 1-17 B	819	42.7	0.5	1.709	0.012	2.717	0.011	0.629	0.005	<b>95.1</b>	2.2	3.25	0.03
CAN 1-17 D	840	50.0	0.8	1.744	0.012	2.727	0.003	0.639	0.004	<b>97.2</b>	2.0	3.27	0.02
CAN 1-18	850	59.6	1.2	1.698	0.013	2.671	0.005	0.636	0.005	<b>96.5</b>	2.2	3.20	0.02
CAN 1-18 B	876.5	58.4	1.0	1.709	0.012	2.650	0.006	0.645	0.005	<b>98.8</b>	2.2	3.18	0.02
CAN 1-19 A	913	53.0	0.9	1.785	0.013	2.751	0.005	0.649	0.005	<b>99.4</b>	2.2	3.32	0.02
CAN 1- 22 R	1050	56.7	0.6	1.726	0.002	2.727	0.005	0.633	0.005	<b>96.0</b>	2.0	3.27	0.02
K 22	1050	62.1	n.d.	1.600	0.005	2.583	0.006	0.620	0.003	<b>93.3</b>	1.1	3.06	0.01
CAN 1- 24 R	1150	71.3	0.1	1.727	0.002	2.765	0.004	0.625	0.005	<b>94.4</b>	2.0	3.30	0.02
K 28	1350	59.1	n.d.	1.746	0.006	2.698	0.008	0.647	0.004	<b>99.1</b>	1.3	3.25	0.02
K 31	1500	67.2	n.d.	1.821	0.006	2.712	0.007	0.671	0.004	<b>104.6</b>	1.3	3.30	0.01

Table. SI2 cont'd: Cango Caves speleothem U-series dating results. Activity ratios calculated using the decay constants for  $^{234}\text{U}$  and  $^{230}\text{Th}$  determined by Cheng et al. (2013). Values/yr:  $^{234}\text{U}$  ( $2.8222 \pm 0.0030$ )E-6 and  $^{230}\text{Th}$  ( $9.1706 \pm 0.01335$ )E-6. For samples with significant Th/U ratios (Table B), corrections applied in Table A are based on the assumption that the "detrital fraction" has a Th/U ratio similar to that of average continental crust (4.2) and has U-series nuclides in secular equilibrium. Detrital fractions rarely have Th/U ratios lower than 4.2, and these corrections are the maximum to be expected.

Sample name	Dist, mm	ppb U	ppb Th	atomic		Activity ratios		$(^{234}\text{U}/^{238}\text{U})$	$\pm 1\text{SE}$
				$^{232}\text{Th}/^{238}\text{U}$	$^{238}\text{U Fr detrital}$	$(^{230}\text{Th}/^{238}\text{U})$	$\pm 1\text{SE}$		
CAN 1- 1	0	68.7	7.4	0.111	0.0278	1.169	0.001	2.950	0.015
CAN 1-3	100	76.8	2.6	0.034	0.0086	1.385	0.001	3.079	0.005
CAN 1- 7	300	44.0	3.4	0.079	0.0197	1.465	0.009	2.621	0.006
CAN 1-8	350	36.2	2.3	0.066	0.0164	1.481	0.003	2.660	0.006
CAN 1-15 B	722	55.3	10.0	0.187	0.0466	1.656	0.012	2.635	0.007
CAN 1-16	750	56.3	4.4	0.082	0.0204	1.671	0.012	2.665	0.004



U/Th ages (Table SI2) from CAN1 ranged from  $38.7 \pm 0.9$  ka (0 mm) to  $104.6 \pm 1.3$  ka (at 1500 mm). Some age reversals do exist, and a Bayesian technique (rbacon v.2.4.3; Blaauw and Christen, 2011) was used to create an age model that incorporated all of the available data (Fig. SI2).

Figure. SI2: Speleothem CAN1 age-depth model, established using rbacon v.2.4.3 (Blaauw and Christen, 2011).

### Isotopic equilibrium

The  $\delta^{18}\text{O}$  values of authigenic carbonate depend on the temperature of precipitation in the cave and the  $\delta^{18}\text{O}$  value of the water from which the calcite precipitates. It is also important that isotope equilibrium be maintained. In cases where the correlation between  $\delta^{13}\text{C}$  and  $\delta^{18}\text{O}$  values is significant, it is probably due to kinetic effects related to evaporation, and there is limited relationship between temperature and  $\delta^{18}\text{O}$  value. This situation is typical in carbonate taken from the flanks of speleothems (Hendy, 1971). For CAN1, there is no correlation between  $\delta^{13}\text{C}$  and  $\delta^{18}\text{O}$  values (Fig. SI3), which is consistent with precipitation of calcite in isotope equilibrium.

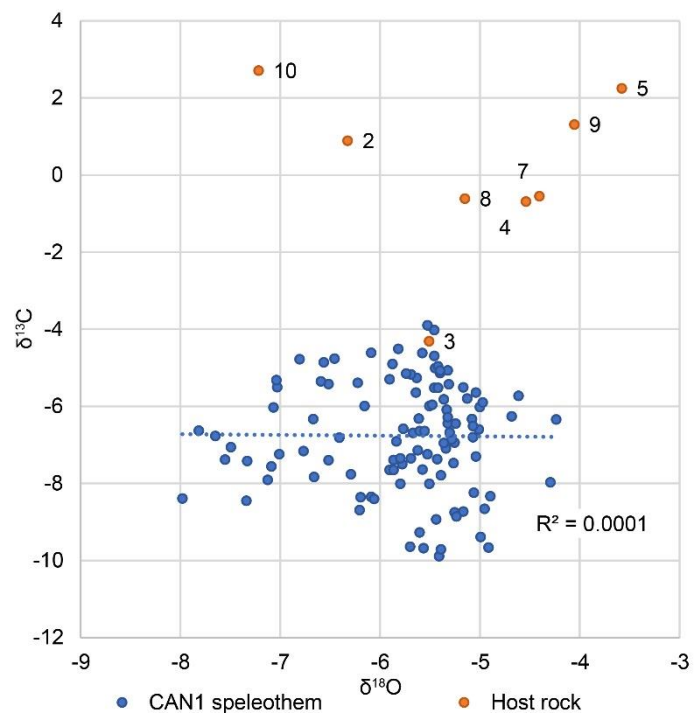


Figure. SI3: Speleothem CAN1 calcite and host rock  $\delta^{13}\text{C}$  and  $\delta^{18}\text{O}$  values. Lack of correlation between CAN1  $\delta^{13}\text{C}$  and  $\delta^{18}\text{O}$  indicates the calcite precipitated in isotopic equilibrium.

### The $\delta^{13}\text{C}$ and $\delta^{18}\text{O}$ values and composite model development

The  $\delta^{13}\text{C}$  values of the samples ( $n=112$ ) vary between  $-3.9\text{‰}$  and  $-9.89\text{‰}$ , and the  $\delta^{18}\text{O}$  between  $-4.24\text{‰}$  and  $-7.98\text{‰}$  relative to the Vienna PeeDee Belemnite (VPDB) standard (Fig SI4). Kinetic fractionation during crystallization of calcite leads to strong correlation between  $\delta^{13}\text{C}$  and  $\delta^{18}\text{O}$  values, and it is clear that no such correlation exists (Fig SI3). Whereas the  $\delta^{13}\text{C}$  values from CAN1 exhibit a high signal-to-noise ratio, the  $\delta^{18}\text{O}$  values are more variable, and were smoothed using a 3-point moving average to reduce noise.

To maximise the utility of the CAN1 data and their integration into the aggregate regional dataset, the data were used as the basis for the creation of composite records integrating comparable data from Efflux Cave (Braun et al., 2020), previously published data from the Cango Caves (Talma and Vogel, 1992) and, in the case of the  $\delta^{13}\text{C}$  data, data from the Seweweekspoort rock hyrax middens (Chase et al., 2017). The composite records (referred to hereafter as Cape Fold Composites; CFC) were created to obtain a coherent signal from the aggregated data (Fig. SI5, 6).

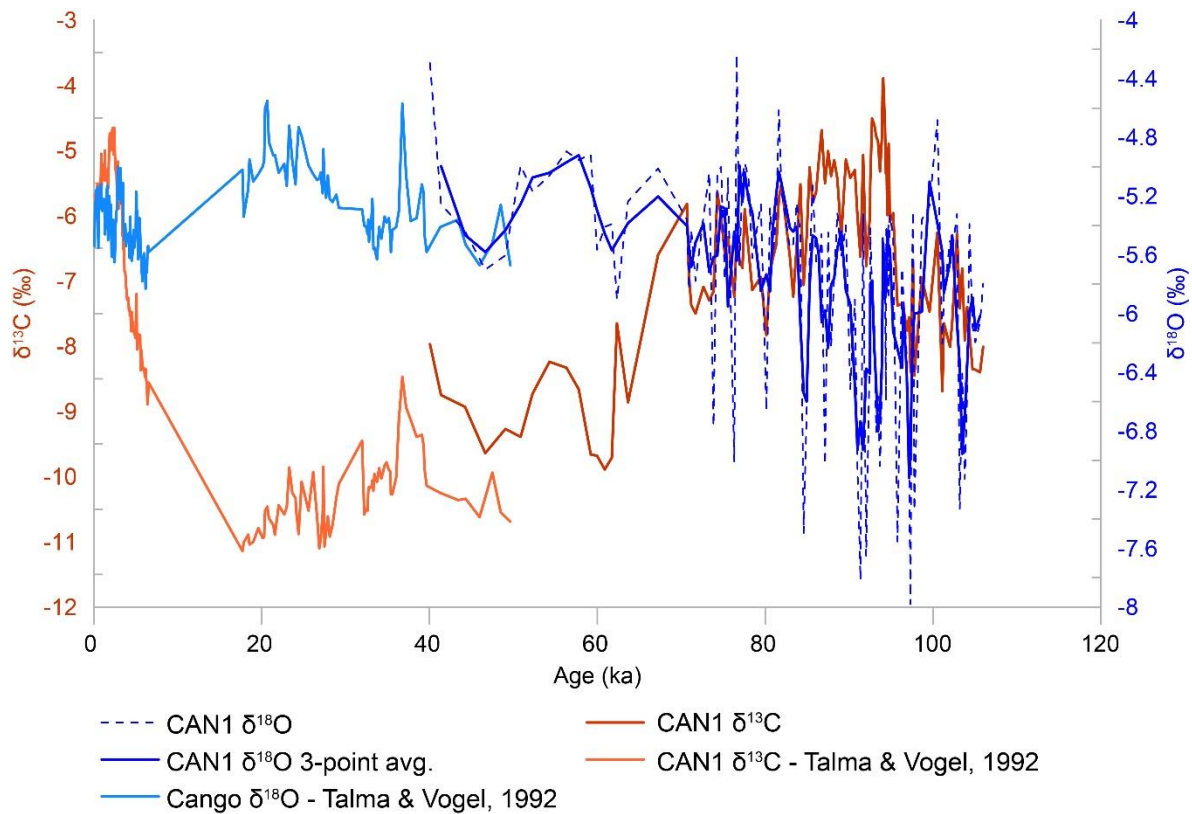


Figure. SI4: Oxygen and carbon isotope records from the Congo Caves, including the CAN1 data presented in this paper and the data of Talma and Vogel (1992).

The speleothem  $\delta^{13}\text{C}$  records reflect changes in the vegetation specific to each site/record, including the potential presence of micro-scale vegetation mosaics that may result in significant differences in the  $\delta^{13}\text{C}$  content of individual speleothems from the same cave, as is the case in Efflux Cave (Braun et al., 2020). It is important to note that while individual speleothem  $\delta^{13}\text{C}$  contents may differ, and the amplitudes of the signals expressed may vary (both as a function of the vegetation present in the drip water source locale), the sign of the signal – reflecting the changes in climate that drive vegetation response – is generally consistent between the records considered here, indicating that a climate signal can be derived from the data. To accurately define this signal at the regional scale, it is necessary to apply scaling transformations to individual records. The Congo Caves speleothems indicate similar  $\delta^{13}\text{C}$  values and amplitudes, and, based on the difference of the mean values of the overlapping portions, a simple  $x-1.1968$  transformation was applied to the CAN1  $\delta^{13}\text{C}$  record to align it with the Congo Caves speleothem  $\delta^{13}\text{C}$  record of Talma and Vogel (1992), creating a Congo Caves composite  $\delta^{13}\text{C}$  record. To account for regional differences in vegetation composition, and render the Efflux Cave  $\delta^{13}\text{C}$  records comparable both with each other and with the Congo Caves composite record, reduced major axis regression (RMA) was used between each of the Efflux Cave speleothem  $\delta^{13}\text{C}$  records and the overlapping section of the Congo Caves composite  $\delta^{13}\text{C}$  record to estimate scaling transformations to minimize the Euclidean distance between the datasets (for speleothem 142843,  $(x*0.39647)-6.9412$ ; for speleothem 142848,  $(x*1.354)-4.9988$ ; speleothems 142847 and 142849 were combined prior to scaling to improve overlap with Congo Caves composite,  $(x*0.74706)-4.1018$ ; speleothem 142846 does not overlap with

any other record, but based on similarities in value and amplitude of variability with speleothems 142847 and 142849 the same  $(x*0.74706)-4.1018$  transform was applied). Based on the similarities between the Cango Caves speleothem  $\delta^{13}\text{C}$  record of Talma and Vogel (1992) and the Seweweekspoort rock hyrax midden  $\delta^{13}\text{C}$  record (Chase et al., 2017), we have used this latter record to span the hiatus present in the Talma and Vogel record. As with the Efflux Cave data, RMA regression between the Seweweekspoort  $\delta^{13}\text{C}$  record and the Cango Caves composite  $\delta^{13}\text{C}$  record was used to estimate a scaling transformation  $((x*1.642)+33.94)$  for the Seweweekspoort data. Finally, the Cango Caves, Efflux Cave and Seweweekspoort records were compiled, sorted by age, normalized using a standard score (to avoid confusion regarding reporting of corrected  $\delta^{13}\text{C}$  data) and, to improve the signal to noise ratio (Fig. SI5).

The speleothem  $\delta^{18}\text{O}$  records were combined to create a composite record using the same process that was applied to the  $\delta^{13}\text{C}$  records, with the same goal of obtaining a record that reflects regional changes in climate with a high signal to noise ratio. As the CAN1  $\delta^{18}\text{O}$  record expresses particularly high frequency variability prior to ~70 ka (likely a product of the increase in tropical influence described in the main text) a 3-point moving average was applied as an initial step to improve the signal to noise ratio. The CAN1 speleothem and that analysed by Talma and Vogel (1992) indicate similar  $\delta^{18}\text{O}$  values and amplitudes for the 40-50 ka period during which they overlap, and the records were simply compiled and sorted by age and normalized using a standard score to obtain a composite record. Determined by similarities in terms of values and amplitudes of variability between Efflux Cave speleothem  $\delta^{18}\text{O}$  records 142843, 142846, 142847 and 142849 were compiled and sorted by age, to create a partial composite. The  $\delta^{18}\text{O}$  record from speleothem 142848 exhibits a pattern of overall variability similar to the other Efflux Cave  $\delta^{18}\text{O}$  records, but at slightly higher values and reduced amplitude of variability. RMA regression was used to estimate a scaling transformation  $((x*2.3855)+4.9234)$  to minimize the Euclidean distance between the 142848  $\delta^{18}\text{O}$  record and the Efflux Cave partial composite. With this transformation applied, the 142848  $\delta^{18}\text{O}$  record was compiled with the other Efflux Cave  $\delta^{18}\text{O}$  records, and the aggregate was sorted by age and normalized using a standard score. RMA regression was then applied to the overlapping sections of the Cango Caves and Efflux Cave composite  $\delta^{18}\text{O}$  records, with a scaling transform of  $(x*0.61024)+0.16217$  being applied to the Efflux Cave composite to create a coherent regional CFC composite  $\delta^{18}\text{O}$  record (Fig. SI6).

Both the CFC  $\delta^{13}\text{C}$  and  $\delta^{18}\text{O}$  records were smoothed using a Gaussian kernel method with a kernel width  $\sigma = 0.3$  ka. These composites are plotted with 95% confidence intervals for the reconstructions in Fig. SI5,6. Uncertainties associated with age estimates are indicated in Table SI2 and the original papers describing the Efflux Cave speleothems (Braun et al., 2020) and the speleothem from the Cango Caves analysed by Talma and Vogel (1992; Vogel and Kronfeld, 1997).

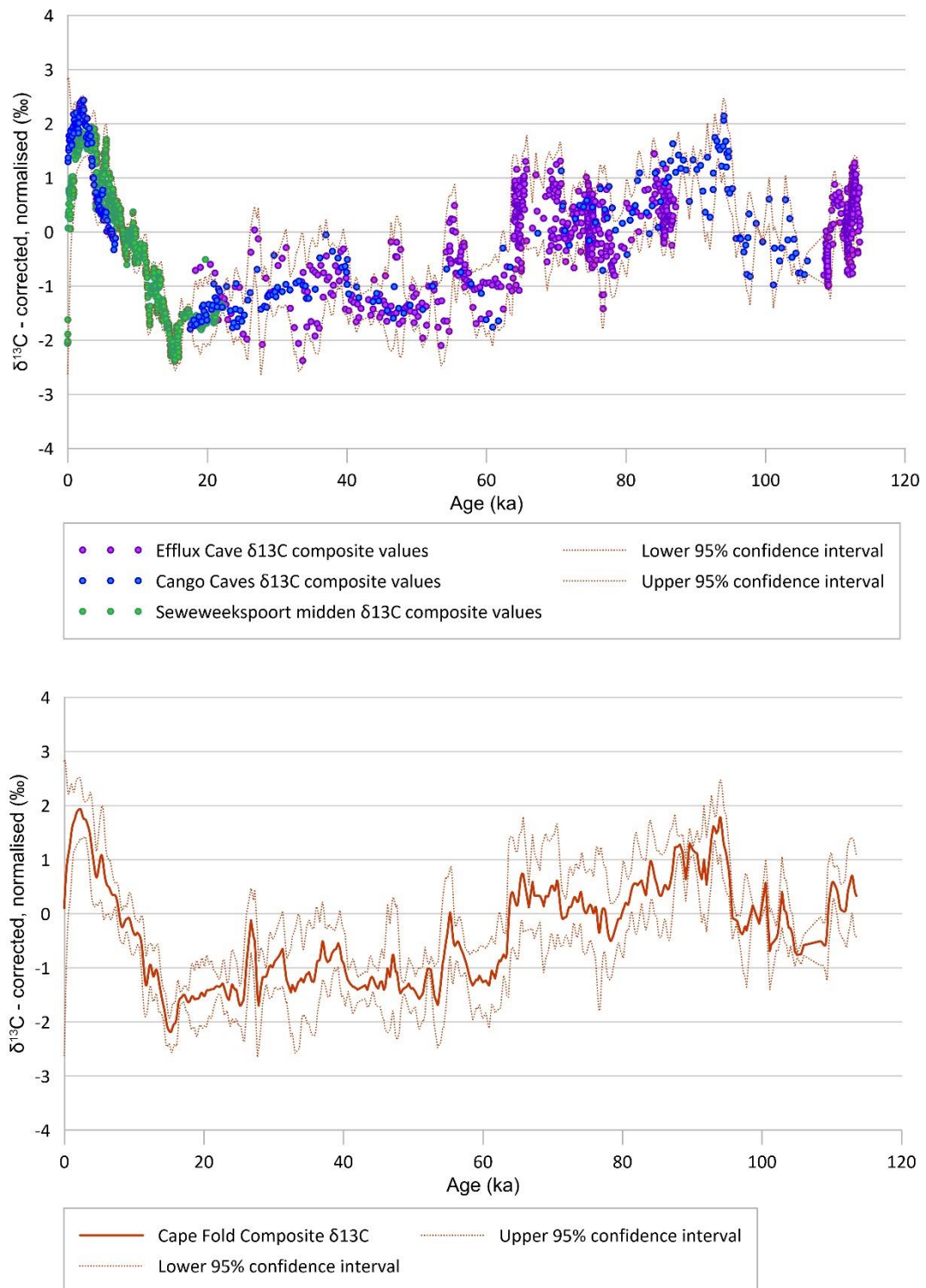


Figure. SI5: Cape Fold Composite  $\delta^{13}\text{C}$  record: Component and composite stable carbon isotope records from the Cango Caves - CAN1 and the data of Talma and Vogel (1992), Efflux Cave (Bar-Matthews et al., 2010; Braun et al., 2020), and the Seweweekspoort rock hyrax middens (Chase et al., 2017). Composite records and 95% confidence intervals for the composite were established using a Gaussian kernel method with a kernel width  $\sigma = 0.3$  ka.

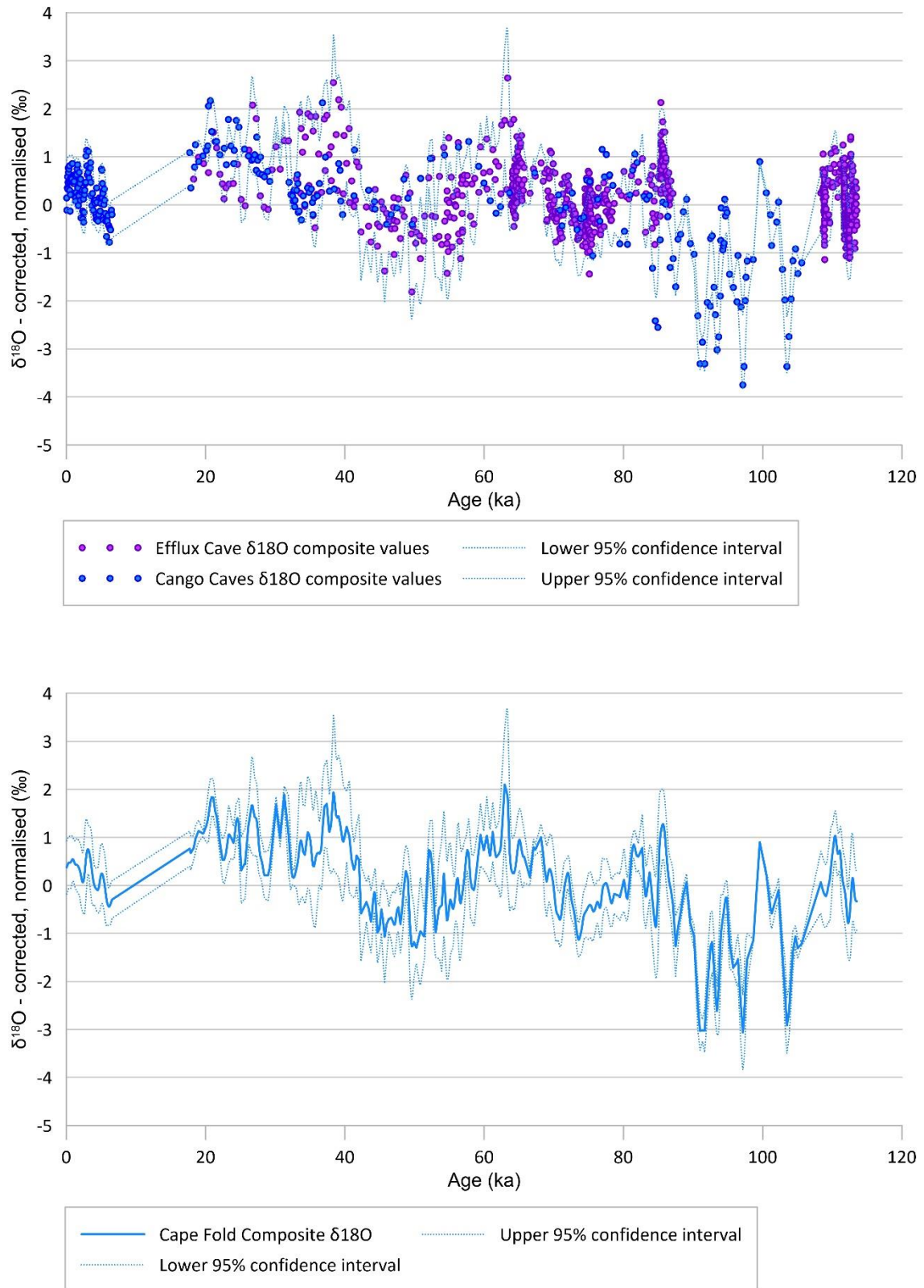


Figure. SI6: Cape Fold Composite  $\delta^{18}\text{O}$  record: Component and composite stable oxygen isotope records from the Cango Caves - CAN1 and the data of Talma and Vogel (1992) - and Efflux Cave (Bar-Matthews et al., 2010; Braun et al., 2020). Composite records and 95% confidence intervals for the composite were established using a Gaussian kernel method with a kernel width  $\sigma = 0.3$  ka.

## REFERENCES

- South African Spelaeological Association, 1978, Cango Cave - The combined 1956 & 1978 surveys by the S.A. Spelaeological Association (Cape Section).
- Bar-Matthews, M., Marean, C. W., Jacobs, Z., Karkanas, P., Fisher, E. C., Herries, A. I. R., Brown, K., Williams, H. M., Bernatchez, J., Ayalon, A., and Nilssen, P. J., 2010, A high resolution and continuous isotopic speleothem record of paleoclimate and paleoenvironment from 90 to 53 ka from Pinnacle Point on the south coast of South Africa: *Quaternary Science Reviews*, v. 29, no. 17-18, p. 2131-2145.
- Blaauw, M., and Christen, J. A., 2011, Flexible paleoclimate age-depth models using an autoregressive gamma process: *Bayesian Analysis*, v. 6, no. 3, p. 457-474.
- Braun, K., Bar-Matthews, M., Matthews, A., Ayalon, A., Zilberman, T., Cowling, R. M., Fisher, E. C., Herries, A. I. R., Brink, J. S., and Marean, C. W., 2020, Comparison of climate and environment on the edge of the Palaeo-Agulhas Plain to the Little Karoo (South Africa) in Marine Isotope Stages 5–3 as indicated by speleothems: *Quaternary Science Reviews*, v. 235, p. 105803.
- Chase, B. M., Chevalier, M., Boom, A., and Carr, A. S., 2017, The dynamic relationship between temperate and tropical circulation systems across South Africa since the last glacial maximum: *Quaternary Science Reviews*, v. 174, p. 54-62.
- Cheng, H., Lawrence Edwards, R., Shen, C.-C., Polyak, V. J., Asmerom, Y., Woodhead, J., Hellstrom, J., Wang, Y., Kong, X., Spötl, C., Wang, X., and Calvin Alexander, E., 2013, Improvements in <sup>230</sup>Th dating, <sup>230</sup>Th and <sup>234</sup>U half-life values, and U–Th isotopic measurements by multi-collector inductively coupled plasma mass spectrometry: *Earth and Planetary Science Letters*, v. 371-372, p. 82-91.
- Doel, S. L., 1995, Cango Caves stable isotope stratigraphy [BSc Honours: University of Cape Town].
- Hendy, C. H., 1971, The isotopic geochemistry of speleothems--I. The calculation of the effects of different modes of formation on the isotopic composition of speleothems and their applicability as palaeoclimatic indicators: *Geochimica et Cosmochimica Acta*, v. 35, no. 8, p. 801-824.
- Talma, A. S., and Vogel, J. C., 1992, Late Quaternary paleotemperatures derived from a speleothem from Cango Caves, Cape Province, South Africa: *Quaternary Research*, v. 37, no. 2, p. 203-213.
- Vogel, J. C., and Kronfeld, J., 1997, Calibration of radiocarbon dates for the Late Pleistocene using U/Th dates on stalagmites: *Radiocarbon*, v. 39, no. 1, p. 27-32.